Nano Energy 101 (2022) 107617

Contents lists available at ScienceDirect

Nano Energy

journal homepage: www.elsevier.com/locate/nanoen

Engineering high-emissive silicon-doped carbon nanodots towards efficient large-area luminescent solar concentrators

Xiao Gong [a,*], Shuyang Zheng [a], Xiujian Zhao [a], Alberto Vomiero [b,c,**]

[a] State Key Laboratory of Silicate Materials for Architectures, Wuhan University of Technology, Wuhan 430070, PR China
[b] Division of Materials Science, Department of Engineering Sciences and Mathematics, Luleå University of Technology, Luleå 971 87, Sweden
[c] Department of Molecular Sciences and Nanosystems, Ca' Foscari University of Venice, Via Torino 155, Mestre, Venezia 30172, Italy

ARTICLE INFO

Keywords:
Luminescent solar concentrators
Silicon-doped carbon nanodots
High-performance
Power conversion efficiency

ABSTRACT

Luminescent solar concentrators (LSCs) are devices that can collect sunlight from a large area, concentrating it at the borders of the slab, to achieve efficient photovoltaic conversion when small area solar cells are placed at their edges, realizing building-integrated photovoltaics. Efficient luminophores in terms of high luminescence quantum yield are needed to obtain high-performance LSCs. A key point is the ability to engineer the Stokes shift (i.e. the difference between the maximum of the absorption and emission spectra), to minimize reabsorption processes. In this work, we report novel silicon-doped carbon nanodots (Si-CDs) with an ultrahigh quantum yield (QY) up to 92.3% by a simple hydrothermal method. Thin-film structured LSCs ($5 \times 5 \times 0.2$ cm^3) with different concentrations of Si-CDs are prepared by dispersing the Si-CDs into polyvinyl pyrrolidone (PVP) matrix, and the optimal power conversion efficiency (PCE) of LSCs can be as high as 4.36%, which is nearly 2.5 times higher than that prepared with silicon-undoped CDs. This Si-CDs/PVP film LSC has a high QY of 80.5%. A large-area LSC (15×15 cm^2) is also successfully fabricated, which possesses a PCE of 2.06% under natural sunlight irradiation (35 $mW \cdot cm^{-2}$), one of the best reported values for similar size LSCs. The efficient Si-CDs as luminescent substances for high-efficiency large-area LSCs will further give an impetus to the practical exploitation of LSCs.

1. Introduction

Currently, the climate and environmental problems caused by the excessive use of fossil energy have led to a growing demand for renewable and clean energy. Solar energy is considered as a renewable and clean energy source, which can effectively alleviate energy shortage, and environmental and climate change issues [1–4]. Although solar technologies have been widely used, it is still a great challenge to reduce the cost of electricity generated by the solar cells. Meanwhile, it is also hard to further boost the power conversion efficiency (PCE) of solar cells. Luminescent solar concentrators (LSCs) are large-area sunlight collectors, which enable the conversion of sunlight to electricity by photovoltaics (PVs) [1,5,6]. Typically, an LSC consists of a transparent waveguide substrate and a luminescent layer covering the surface of the substrate or embedded in it. The luminophore absorbs part of the sunlight and re-emits photons at longer wavelengths. Due to the total internal reflection, the emitted photons are waveguided to the edges of the waveguide substrate and further converted to electricity by the solar cells mounted at the slab edges [1,6,7]. LSCs can collect and redirect the sunlight from a large area to increase the conversion efficiency and reduce the area of the solar cells, thus reducing the cost of the electricity and increasing the potential of practical application of energy conversion systems. In addition, LSCs can be lightweight and semi-translucent with tunable color, which support their use in building-integrated photovoltaics (BIPVs) [1,5,7–19]. However, many issues still exist that block the practical applications of LSCs so far [20]. The most critical one is the strong reabsorption energy loss of the luminescent material, which hinders the possibility of large-area LSC applications due to the overlap of absorption and emission spectra, resulting in heavy reabsorption losses [1,6,7]. Second, it is also important to reduce the efficiency losses due to parasitic absorption and scattering at optical defects and surface reflection at the lightguide surface [21]. The optical efficiency of LSCs depends not only on the optical properties of the luminescent materials, but also on the optical properties of the waveguide material. Therefore,

* Corresponding author.
** Corresponding author at: Division of Materials Science, Department of Engineering Sciences and Mathematics, Luleå University of Technology, Luleå 971 87, Sweden.
E-mail addresses: xgong@whut.edu.cn (X. Gong), alberto.vomiero@ltu.se (A. Vomiero).

https://doi.org/10.1016/j.nanoen.2022.107617
Received 29 April 2022; Received in revised form 25 June 2022; Accepted 17 July 2022
Available online 19 July 2022

there is an urgent need to develop efficient fluorophores with a broad absorption spectrum, high quantum yield (QY), small overlap between absorption and emission spectra (i.e. large Stokes shift (SS), the energy difference between the position of the absorption and emission maxima), and good stability, as well as the selection of suitable substrate materials [6].

Various luminescent materials have been used as fluorophores for LSCs, such as organic dyes [22–25], aggregation-induced emission (AIE) molecules [26], metal nanoclusters [27,28], inorganic quantum dots [7,12,13,29–32] and perovskite nanocrystals [33–35]. Compared with inorganic quantum dots containing toxic Pb or Cd, or expensive rare earth elements [13,14,33,36], carbon dots (CDs) are of great interest due to their easy synthesis, low cost, green and non-toxic composition [11,37–42]. CDs have tunable absorption and emission spectra, high absorption coefficients, high photoluminescence QYs and excellent photostability [37–40,43,44]. For example, in 2017, N-doped CDs were used for the first time in single-layer LSCs with a lateral size of 2×2 cm^2 [45]. Based on this, several different luminescent CDs have been applied to large-area single-layer LSCs [46]. Recently, Zhao et al. synthesized CDs with a high QY (65%) and large Stokes shift (0.53 eV) based on a vacuum heating method and prepared large-area LSCs (15×15 cm^2) with external optical efficiency of 2.2% [47]. However, this synthesis method involves the use of vacuum. Thus, it is still a big challenge to synthesize CDs with high QY for high-efficiency LSCs through simple techniques.

In this work, we report a high-efficiency large-area LSC prepared from silicon-doped carbon nanodots (Si-CDs). Compared with Si-undoped CDs, the luminescence intensity of Si-CDs and the performance of the as-prepared LSCs are greatly improved. Novel green emissive Si-CDs with QY up to 92.3% were synthesized by a one-step hydrothermal method using rhodamine B (RhB) and sodium metasilicate as precursors. The LSCs were prepared by drop coating the Si-CDs/polyvinyl pyrrolidone (PVP) solution onto glass. The as-prepared large-area LSCs (15×15 cm^2) based on the Si-CDs exhibited a PCE of 2.06% under natural sunlight irradiation (35 mW·cm^{-2}), which is one of the best values reported in the literature for similar size LSCs, after coupling to a Si solar cell on the slab edge.

2. Results and discussion

2.1. Synthesis and structure of the Si-CDs

Si-CDs were synthesized via a hydrothermal method using RhB and sodium metasilicate as precursors and water as solvent (Fig. 1). The morphology and structure of the Si-CDs were characterized by transmission electron microscope (TEM) and X-ray diffraction (XRD). The TEM image (Fig. 2a) shows that Si-CDs have uniform quasi-spherical shapes with sizes varying from 1.7 to 3.5 nm (average size ~ 2.7 nm) (Fig. S1). The lattice spacing of 0.21 nm (inset of Fig. 2a) corresponds to (100) lattice spacing of graphene [48]. From the XRD patterns (Fig. 2b), a broad diffraction band at 23.7° and a single diffraction peak at 29.4° could be ascribed to disordered carbon atoms and the (002) graphite lattice, respectively, which are very different from the crystalline structure of the RhB precursor [49]. The chemical structure of Si-CDs was characterized by Fourier-transform infrared spectroscopy (FT-IR) (Fig. 2c). In the FT-IR spectrum of RhB, the peak at 1695 cm^{-1} indicates the presence of C═O from the carboxyl group; the peak at 1637 cm^{-1} indicates the presence of C═N; the peak at 1585 cm^{-1} is attributed to the stretching vibrations of C═C bonds, and the peak at 1332 cm^{-1} is assigned to the N-aryl stretching vibrations. Differently from that of RhB, Si-CDs exhibit characteristic peaks of O−H at 3436 cm^{-1}, COO^- at 1390 cm^{-1} and Si−O at 1103 and 1024 cm^{-1} [50,51].

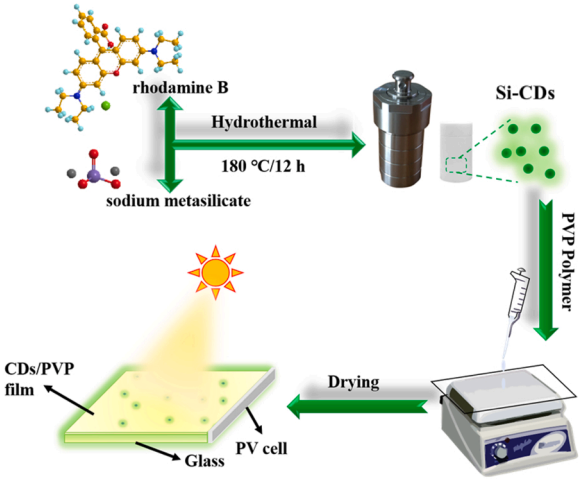

Fig. 1. Schematic diagrams for the synthesis of Si-CDs and LSC preparation procedure.

The X-ray photoelectron spectroscopy (XPS) spectrum indicates the presence of C 1 s, N 1 s, O 1 s and Si 2p at 285, 532, 399 and 102 eV binding energy, respectively, with the corresponding contents of C, N, O and Si in Si-CDs equal to 63.1%, 1.9%, 25.7% and 9.3%, respectively (Fig. 2d). High-resolution XPS spectra depict more details about the chemical bonds of these elements (Fig. S2). The high-resolution spectrum of C 1 s reveals that Si-CDs contain C-C/C═C (284.8 eV), C-N/C-O (286.3 eV) and C═O (288.4 eV). The high-resolution spectrum of N 1 s can be decomposed into four peaks: pyridinic N (399.1 eV), amino N (400 eV), pyrrolic N (401.1 eV) and graphitic N (403 eV). The high-resolution spectrum of O1s can be decomposed into three peaks: Si-O (530.8 eV), C-O (532 eV) and C═O (535.7 eV). The high-resolution spectrum of Si 2p can be decomposed into two peaks: Si-C (102.2 eV) and O-Si-O (103.1 eV), which is consistent with the FT-IR spectral results [51].

2.2. Optical properties of the Si-CDs

The optical properties of Si-CDs were analyzed by UV–vis absorption spectra and steady-state photoluminescence (PL) spectra at room temperature. As shown in Fig. 3a, the Si-CDs dispersed in aqueous solution have two distinct absorption characteristic peaks at 240 nm and 490 nm, which can be attributed to the π-π * transition and n-π * transition of surface states related to C═O, respectively. Si-CDs have a single emission peak at 510 nm under excitation at 490 nm. With increasing excitation wavelength, in the range 420–490 nm, Si-CDs exhibit excitation-independent emission (Fig. 3b). It indicates that the emission in Si-CDs originates from deexcitation from a single energy state. In addition, we measured the transient fluorescence decay of Si-CDs. Fig. 3c and d show the fluorescence behaviors of Si-CDs on the nanosecond time scale with an average lifetime of 4.8 ns and 4.5 ns under excitation at 343 nm and 490 nm, respectively. These lifetime values are within the typical range of the CDs, indicating that the luminescent recombination center is close to band gap. More notably, the QY of Si-CDs is as high as 92.3% (Fig. S3a), suggesting that the nonradiative transition seldom occurs in the Si-CDs [52]. It is found that sodium metasilicate as a dopant can improve the QY of CDs. First, the introduction of silicon can create a new surface state (the so-called silicon state) that traps electrons, increases radiative recombination, and suppresses nonradiative recombination. Second, silicon dopants acting as electron donors can increase the electron cloud density, thereby increasing the probability of electron-hole radiative recombination. Third, the functional groups can act as surface passivators, greatly preventing the vibration, rotation, and aggregation of CDs, ultimately reducing nonradiative processes [53].

2.3. Efficiency of the film LSCs based on Si-CDs

We prepared a series of single-layer film-structured LSCs by drop

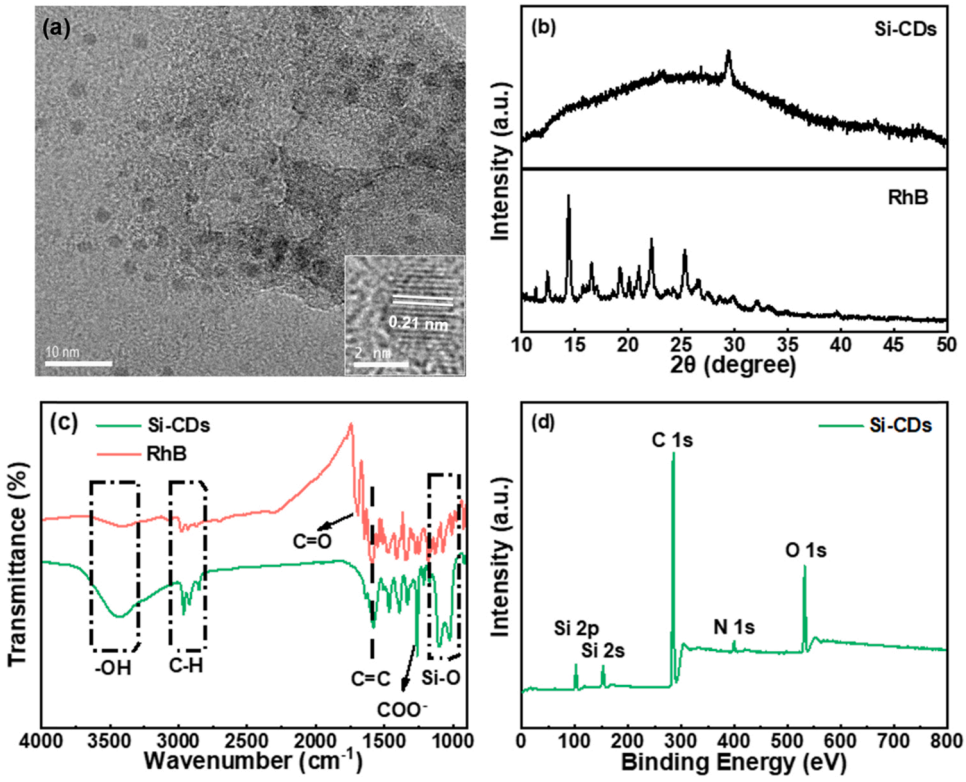

Fig. 2. (a) Typical TEM image of Si-CDs. The inset is the HRTEM image. XRD spectrum (b), FT-IR spectrum (c) and XPS spectrum (d) of Si-CDs.

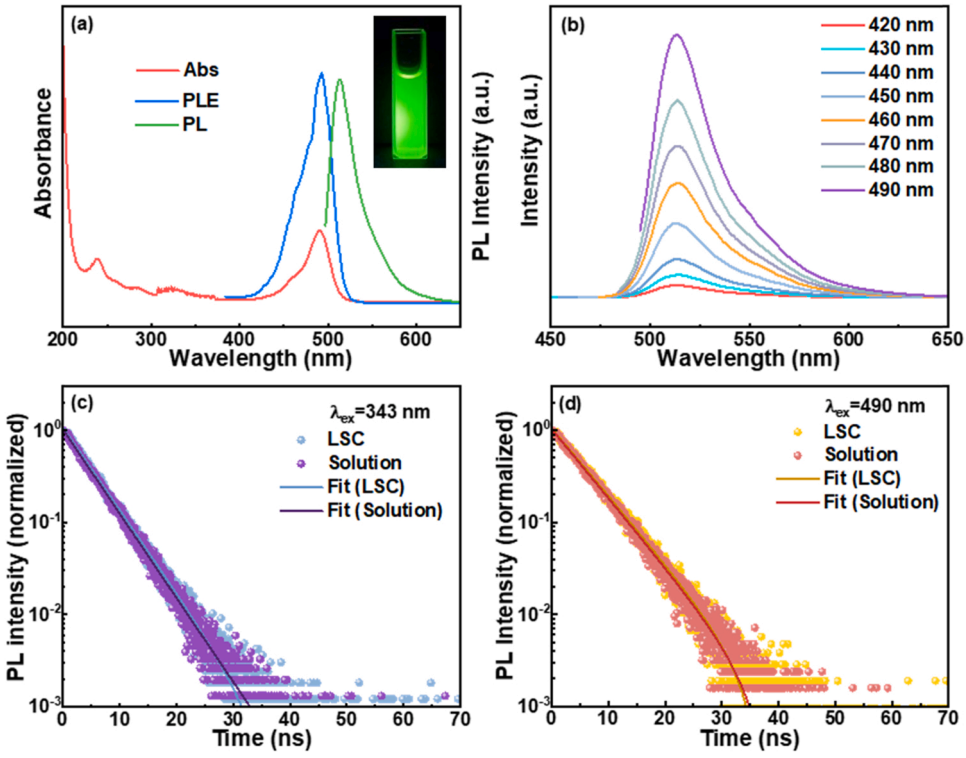

Fig. 3. (a) The absorption, PLE and PL spectra of Si-CDs in aqueous solution. (b) The PL spectra of Si-CDs under different excitation wavelengths. The emission decay from Si-CDs and the LSC (the concentration of Si-CDs is 0.2%) excited with a pulsed laser at 343 nm (c) and 490 nm (d).

casting a PVP-based film on glass with transverse dimensions of 5×5 cm^2 using different concentrations of CD/PVP methanol solutions with 0.05%, 0.10%, 0.15%, 0.20%, 0.25% and 0.30%. For comparison, we also prepared the film LSC with Si-undoped carbon dots under the same conditions (see Experimental Section). The photos of the prepared LSCs under natural light are shown in Fig. 4a. The film-structured LSCs

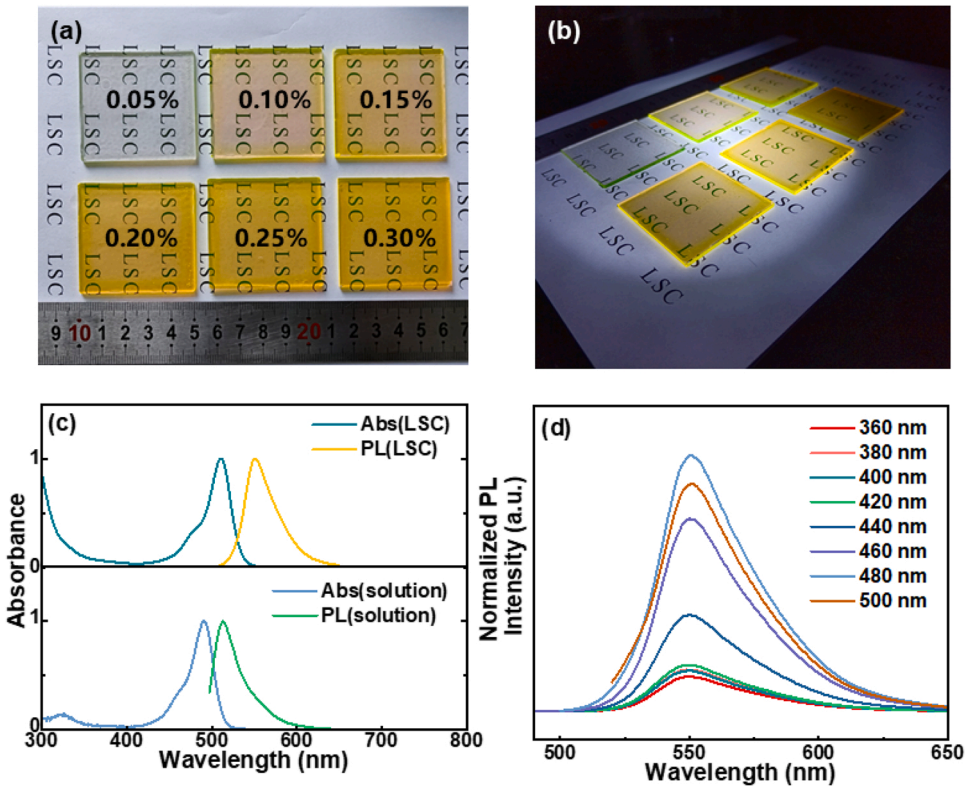

Fig. 4. Photographs of the film LSCs based on Si-CDs under indoor (a) and upon one sun illumination (b). The dimensions of the LSCs were 5 × 5 cm^2. (c) Normalized absorption and emission spectra of the Si-CDs and the film LSC under 490 nm. (d) The PL spectra of the film LSC based on Si-CDs under different excitation wavelengths. The concentration of Si-CDs is 0.20%.

based on Si-CDs are translucent but the transparency decreases with the increase of Si-CDs concentrations, while the "LSC" words at the bottom are still clearly visible. The bright yellow light from the edges of the thin film LSCs can be clearly seen under the illumination of the solar simulator (Fig. 4b). The thicknesses of the film LSCs based on Si-CDs with different concentrations of 0.1%, 0.2% and 0.3% were 74.6 μm, 84.3 μm and 97.4 μm, respectively (Fig. S4). There was an obvious redshift (~ 20 nm) in the absorption and PL emission spectra after embedding the Si-CDs into the PVP polymer matrix (Fig. 4c). This might be due to the more polar environment stabilizing the excited state, leading to a bathochromic shift of the absorption [54]. The red-shift of emission from aqueous solution to thin films may be due to the change of interparticle distance. Since there is a certain degree of overlap between the absorption spectrum and the emission spectrum, as the particle spacing of the carbon dots becomes smaller, the solid-state resonance energy transfer is caused, which makes the emission at long wavelengths relatively enhanced. However, the dilution effect of the aqueous solution can effectively enlarge the inter-particle distance and weaken the energy transfer in the carbon dots, resulting in a relative reduction in long-wavelength emission [55–57]. A significantly broad adsorption peak at 400–550 nm is observed and absorption intensity increases as the Si-CDs concentration increases (Fig. S5a). The PL spectra of LSCs have similar excitation-independent characteristics to Si-CDs, indicating that the PVP polymer does not affect the energy structure of Si-CDs (Fig. 4d). The lifetime of CDs/PVP film is 5.0 ns and 6.0 ns under excitation at 343 nm and 490 nm, respectively, which is a little longer than the lifetime of CDs in the solution (Fig. 3c and d). The as-prepared CDs/PVP film LSC has a high QY of 80.5% at the concentration of 0.2% (Fig. S3b). The acceptable variation of the PL lifetimes and QY before and after polymer encapsulation indicates the optical properties of the CDs does not change very significantly. To understand the pattern of variation of PL property of LSCs, PL spectra of LSCs with different concentrations were measured (Fig. S5b). We found that the PL intensity of LSCs increased significantly with the increase of Si-CDs concentrations.

The functionality of the LSCs was measured according to the latest international standards [58].

The external optical efficiency (η_{opt}) and PCE of the LSC were further measured by coupling the power meter at the edge of the LSC. The η_{opt} can be calculated as follows:[5].

$$\eta_{opt} = \frac{I_{LSC}}{I_{SC} \times G} \times 100\% \quad (1)$$

$$G = \frac{A_{top}}{A_{edge}} \quad (2)$$

Where I_{LSC} is the current of the solar cell mounted on the edge of the LSC and I_{SC} is the current of the solar cell under direct simulated illumination, A_{top} is the top surface area of the LSC and A_{edge} is the surface area of the edges mounted on a solar cell. The PCE can be calculated as follows:

$$\eta = \frac{J_{SC} \times V_{oc} \times FF}{P_0} \quad (3)$$

Where J_{SC} is the short-circuit current density of the solar cell mounted on the LSC and V_{oc} is the open-circuit voltage of solar cell mounted on the LSC, FF is the fill factor and P_0 is the integrated solar power density. The photovoltaic parameters such as V_{oc}, J_{sc}, G, η_{opt} and η for the film LSCs with different concentrations are listed in Table 1. Compared to Si-undoped carbon dots, a dramatic increase in the total emission intensity is observed with Si-CDs (Fig. 5a). PCE is an important parameter to evaluate the optical performance of LSCs. A significant improvement on the PCE with Si-CDs could be observed, i.e. 1.77% for Si-undoped CDs and 4.36% for Si-CDs at the same concentration (Fig. 5b). The photovoltaic performance of the film-structured LSCs based on the different concentrations of Si-CDs is shown in Fig. 5c. The photocurrent density

Table 1
Photovoltaic parameters of the film-structured LSCs based on Si-CDs with different concentrations.

Concentration	J_{sc} (mA cm^{-2})	V_{oc} (V)	FF (%)	G	η_{opt} (%)	η (%)
0.05%	5.0	0.49	72.4	6.25	2.15	1.80
0.10%	8.4	0.50	73.4	6.25	3.60	3.05
0.15%	10.8	0.51	74.3	6.25	4.60	4.15
0.20%	11.3	0.52	74.5	6.25	4.80	4.36
0.25%	10.8	0.52	74.3	6.25	4.65	4.15
0.30%	10.3	0.51	74.3	6.25	4.45	3.95

increases significantly with increasing Si-CDs concentration and then decreases slightly. The best values of V_{oc}, J_{sc}, η_{opt} and η are obtained at 0.52 V, 11.3 mA/cm^2, 4.8% and 4.4%, respectively, when the concentration of Si-CDs in the thin-film LSC is 0.2%. This is because there is a certain overlap between absorption and emission of Si-CDs, and the photons emitted from Si-CDs may be absorbed by themselves. Even if Si-CDs can re-emit new photons after absorbing the emitted photons, since the fluorescence quantum efficiency is smaller than 1, the fluorescence intensity of the edge is definitely smaller, resulting in a loss of the power conversion efficiency.

To study the stability of LSCs, the prepared LSCs were kept for 4 weeks under natural sunlight irradiation conditions (summer, Wuhan, China, the average daily light intensity: ~ 64 mW cm^{-2}, the average daily illumination time: ~ 10.5 h), and we measured the *J-V* characteristic curves of LSCs each week for five consecutive times (Fig. 5d). It is found that the PCE of the thin film LSCs based on Si-CDs does not change significantly, indicating the good stability of the LSCs based on Si-CDs.

To further evaluate the feasibility of large-area thin-film LSCs, we examined the effect of reabsorption for different concentrations of thin-film LSCs. The Stokes shift is often used to quantify and rationalize this loss in LSCs, and it is generally accepted that SS is the key to influence the reabsorption of luminescent material in LSC devices. However, recent literature has demonstrated that the scalability of LSC devices is not necessarily correlated with SS, but depends on the total overlap of the absorption tail shape. Two redefined parameters have been used to better predict the effect of LSC reabsorption on scalability, namely the quality factor (QF) [59] and the overlap integral (OI):[54].

$$QF = \alpha_1/\alpha_2 \tag{4}$$

Where α_1 is the absorption coefficient at the wavelength λ_1 of collected light and α_2 is the absorption coefficient at the emission peak λ_2.

$$OI = \int_0^\infty A(\lambda)\cdot PL^*(\lambda)d\lambda \tag{5}$$

Where $A(\lambda)$ is the absolute absorption spectrum of a luminophore/host composite film, and $PL^*(\lambda)$ is the normalized emission spectrum of the luminophore in the host material. The calculated results of the relevant parameters are listed in Table S1. The QF and OI of LSCs gradually increase with the increase of Si-CDs concentrations, indicating that the influence of Si-CDs reabsorption gradually increases. The absorption peak position of the thin film LSCs remains unchanged, and the absorption coefficient gradually becomes larger. Meanwhile, the emission peak is slightly red-shifted, and the optical efficiency first increases and then decreases. The performance of LSCs is mainly the result of the combined effect of absorption efficiency and reabsorption loss.

Due to the limited reabsorption and scattering losses of small-sized LSCs, their photovoltaic properties are severely overestimated, while practical applications require larger areas to meet life requirements. To get closer to the size of the device for practical applications and to verify whether the Si-CDs are reasonably scalable, we prepared a large-area film LSC with a size of 15 × 15 cm^2 by applying Si-CDs/PVP solution with the optimal concentration dropwise to the glass and then drying it. Fig. 6a and b show the optical photo of the large-area LSC and the photo under the solar light simulator. It can be seen that it maintains excellent translucency and still emits bright light at the edge of the glass despite the nine-fold increase in area. According to the method reported in the literature [47], we set up a distance-dependent PL measurement as shown in Fig. S6b. Usually, the distance-dependent red-shift of PL peak position or the narrowing of PL peak width is due to the reabsorption caused by the overlap between the absorption and emission spectra at

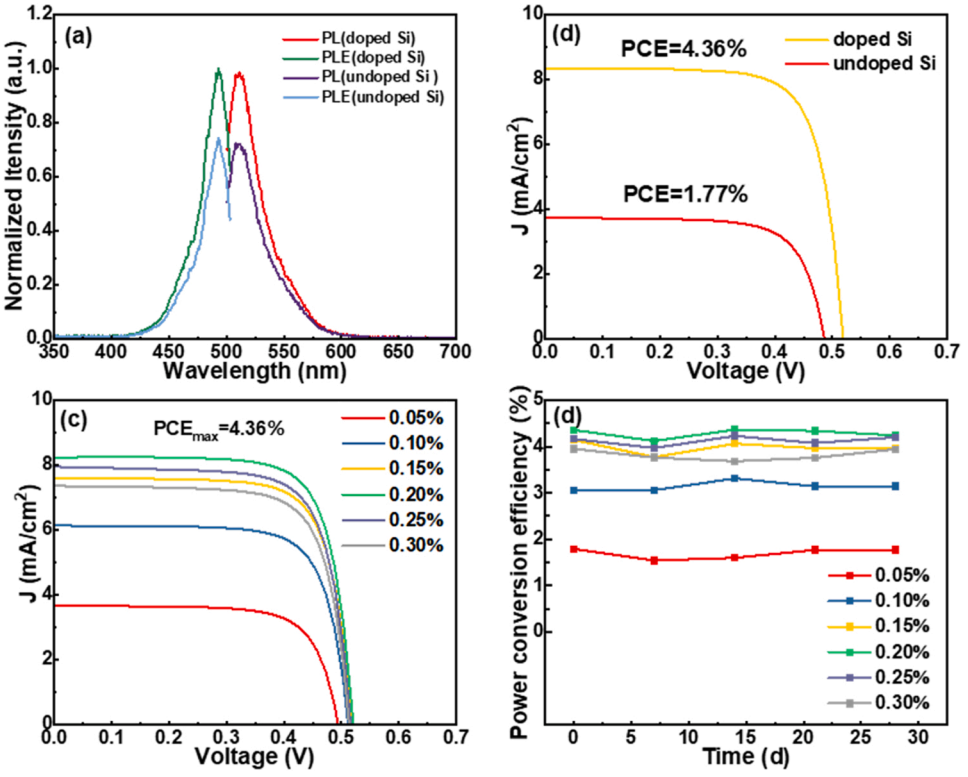

Fig. 5. (a) PL excitation and emission spectra of Si-CDs and Si-undoped CDs (b) J–V response of silicon PVs attached on the edge of the film LSCs based on Si-CDs and Si-undoped CDs (c) *J–V* response of silicon PVs attached on the edge of the film LSCs based on Si-CDs with different concentrations of Si-CDs. (d) Power conversion efficiency of the film LSCs during four-week storage in ambient conditions (under natural sunlight irradiation in Wuhan, China, the average daily light intensity: ~ 64 mW cm^{-2}, the average daily illumination time: ~ 10.5 h).

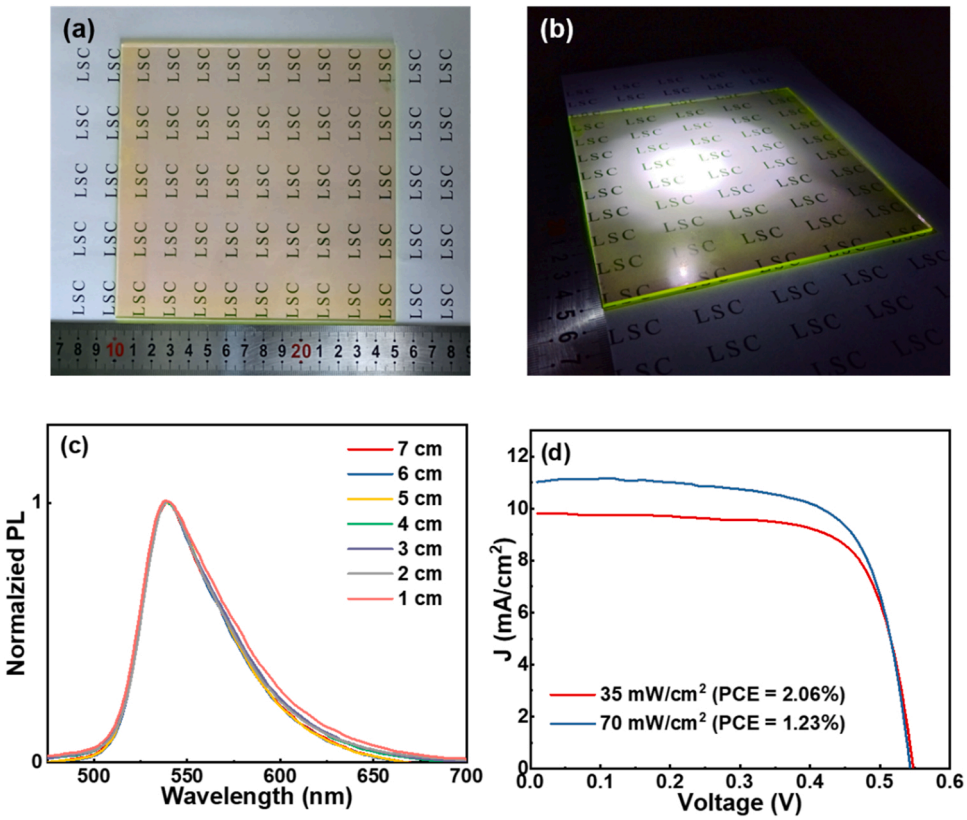

Fig. 6. Photographs of the LSC under indoor (a) and simulated sunlight (b). (c) Normalized PL spectra measured at different optical paths (L, distance between the beam spot and the edge of the LSC in the detector direction) for the film LSC base on Si-CDs. The excitation wavelength was 490 nm. (d) *J–V* response of silicon PVs attached on the edge of the LSC under different natural sunlight intensity (35 and 70 mW·cm^{-2}). The dimensions of the LSC were 15 × 15 × 0.5 cm^3.

the CDs. This phenomenon has been widely reported and used to evaluate the reabsorption energy loss in LSC [43]. As the distance between the light spot and the detector increases, there is almost no redshift of the PL emission peak and a slight narrowing of the PL peak width, as shown in Fig. 6c. The result suggests that this large-area LSC has an acceptable reabsorption loss to meet the scaling needs in practical applications.

The PCE of the LSC was measured by using a calibrated silicon PV cell. The measurement of natural sunlight intensity was performed by using a commercially calibrated Zolix QE-B1 solar cell. Under natural sunlight, the film LSC based on Si-CDs exhibited similar *J-V* behavior to PV (Fig. 6d). The PCE of the LSC (15 × 15 cm^2) is as high as 2.06% upon a natural sunlight intensity of 35 mW·cm^{-2}. At a comparably high natural light intensity (70 mW·cm^{-2}), the LSC still exhibits a PCE of 1.23%, which is relatively higher than the results of other similar studies (Table S2). The lower light intensity leads to a higher PCE, which may be due to the absorption limit of Si-CDs at higher light intensities [47]. This suggests that LSCs based on Si-CDs are well adapted for use in low-light weather.

Compared to the recent work [47], this work shows obvious progress. (1) Novel green emissive Si-CDs were synthesized by a one-step hydrothermal method. The synthesis procedure is facile without vacuum reaction conditions, which is expected to achieve the large-scale preparation of Si-CDs for practical applications. (2) Si-CDs show ultrahigh PLQY over 90%, which is much higher than that of the previous work (~65%) and more appropriate for LSC application. Most importantly, PCE as high as 2.06% of the LSC (15 × 15 cm^2) based on Si-CDs was achieved, which is higher than that of other previous works with the similar sizes. (3) The LSCs based on Si-CDs are highly stable without any noticeable variation in photoluminescence under natural sunlight illumination for over four weeks.

3. Conclusions

In summary, we first synthesized novel Si-CDs with an ultrahigh QY of 92.3% by a hydrothermal method, and then fabricated a series of the thin-film LSCs (5 × 5 cm^2) with different concentrations of Si-CDs. We investigated the photovoltaic properties and reabsorption patterns of the film LSCs with various concentrations. The results show that the PCE first increased and then decreased as the concentration of Si-CDs increased. The optimal performance of LSCs was achieved when the concentration was 0.2%, and the PCE value could reach 4.36%. In addition, the photostability of LSCs is very good. Based on its broad absorption and relatively low reabsorption loss, we applied the Si-CDs to prepare high-performance large-area LSCs (15 × 15 cm^2), which exhibited a PCE of 2.06% under natural sunlight irradiation (35 mW·cm^{-2}) after coupling with a Si solar cell, which is one of the best values reported in the literature for similar size LSCs. The simple synthesis process, low cost and excellent optical properties of Si-CDs pave the way for practical applications of LSCs such as BIPVs.

4. Experimental section

4.1. Materials

Polyvinylpyrrolidone (PVP) K30 (MW: 50,000) and K90 (MW: 1,000,000), sodium metasilicate, rhodamine B, ethanol and methanol were obtained from Aladdin Chemicals Ltd, China. All chemicals were used for purchase.

4.2. Synthesis of Si-CDs

Typically, 20 mg of rhodamine B and 0.5 g of sodium metasilicate were first added to 20 mL of deionized water and sonicated for 10 min to

dissolve them completely. The solution was then transferred to a 25 mL autoclave and maintained at 180 °C for 12 h. After cooling to room temperature, the product was filtered using a 0.22 μm pore size filter to remove the large particles. Then, to remove unreacted small molecules, the product was dialyzed for 24 h using a dialysis bag with a cut-off molecular weight of 500 Da. Finally, the purified solution was dried in an oven to obtain a brown carbon dot powder for further characterization and LSC device preparation.

For comparison, 20 mg rhodamine B was dispersed in 20 mL deionized water with the same amount of sodium carbonate, and then reacted under the same conditions.

4.3. LSCs fabrication

The thin film LSC is prepared by drop coating method. Specifically, Si-CDs methanol solutions (0.2, 0.4, 0.6, 0.8, 1.0 and 1.2 mL) at a concentration of 1.5 mg/mL were mixed with 3 mL of PVP methanol solutions (100 mg/mL PVP K30 and 100 mg/mL PVP K90), respectively. The mixture was stirred for 3 h to obtain a homogeneous clarified solution and sonicated for 10 min to remove air bubbles from the solution. The solution was then applied dropwise to a glass surface measuring 5×5 cm^2 (glass thickness 2 mm) and dried at room temperature until the methanol evaporated completely. For convenience, the six Si-CDs film LSCs thus prepared from 0.2, 0.4, 0.6, 0.8, 1.0 and 1.2 mL were labeled as 0.05%, 0.10%, 0.15%, 0.20%, 0.25% and 0.30%, respectively. The film LSC based on Si-undoped CDs and Large-area LSCs ($15 \times 15 \times 0.5$ cm^3) were prepared at optimal concentration of 0.20% as described above.

4.4. Characterizations

The morphology of Si-CDs was measured via transmission electron microscopy (TEM) using a JEM-2100 F TEM (JEOL, Japan). The scanning electron microscope (SEM) examination of thin-film LSCs was performed using a JSM-7500 F SEM (JEOL, Japan). Fourier transform infrared (FT-IR) spectra were recorded on an FT-IR spectrometer (Nicolet 6700, Thermo Electron Co., USA). X-ray diffraction (XRD) was performed using a D8 Advance diffractometer (Bruker, Germany, Kα = 1.5406 Å). The X-ray photoelectron spectroscopy (XPS) spectra of the samples were recorded using a Thermo Fisher Scientific ESCALAB 250Xi spectrometer equipped (USA). UV–visible absorption spectra of Si-CDs were recorded in solution on a UV-Vis spectrophotometer (UV2700, Shimadzu Corp., Tokyo, Japan). PL spectra of Si-CDs were recorded in solution at room temperature on a fluorescence spectrometer (Agilent Cary Eclipse, USA). The fluorescence delay was achieved by an automatic delay stage (M-ILS300LM, Newport, USA). The intensity of the pump light was directly measured using a power meter (Model 843-R, Newport). The focal size of pump beam (~0.1 mm) was measured using a beam profiler (LBP2-HR-VIS2, Newport, USA). The QY of the film LSC was recorded with an absolute PL quantum yield spectrometer (Hamamatsu Photonics, C9920–02 G) equipped with Xe light source with fiber input optic and an integrating sphere. The measurements were performed in a quartz dish without caps at ambient temperature. The illumination spot was Introduced through an optical fiber with an inner diameter of 3 mm. The surface area of the tested LSC is 5×5 cm^2 and the thickness was relatively uniform. The lightguide edges were not blackened and this edge-emission was collected. Photovoltaic properties of LSCs were obtained with a solar simulator (IV4112, Newport Corp., Irvine, CA, USA) at an intensity of 100 $mW \cdot cm^{-2}$ (1 sun), calibrated through a calibrated silicon solar cell.

CRediT authorship contribution statement

Xiao Gong: Conceptualization, Methodology, Writing – review & editing, Supervision. **Shuyang Zheng:** Data curation, Writing – original draft. **Xiujian Zhao:** Writing – review & editing. **Alberto Vomiero:** Writing – review & editing.

Declaration of Competing Interest

The authors declare that they have no known competing financial interests or personal relationships that could have appeared to influence the work reported in this paper.

Data Availability

Data will be made available on request.

Acknowledgements

This work was supported by the National Natural Science Foundation of China (No. 21774098), and the 111 project (No. B18038). A. Vomiero acknowledges the Kempe Foundation, the Wallenberg Foundation and LTU Labfund for financial support.

Appendix A. Supporting information

Supplementary data associated with this article can be found in the online version at doi:10.1016/j.nanoen.2022.107617.

References

[1] Q. Li, M. Zhou, M. Yang, Q. Yang, Z. Zhang, J. Shi, Induction of long-lived room temperature phosphorescence of carbon dots by water in hydrogen-bonded matrices, Nat. Commun. 9 (1) (2018) 734.
[2] G.J. Liu, B.F. Sun, H.L. Li, Y.Q. Wang, H.G. Zhao, Integration of photoelectrochemical devices and luminescent solar concentrators based on giant quantum dots for highly stable hydrogen generation, J. Mater. Chem. A 7 (31) (2019) 18529–18537.
[3] D. Cambi, J. Dobbelaar, P. Riente, J. Vanderspikken, C. Shen, P.H. Seeberger, K. Gilmore, M.G. Debije, T. Nol, Energy-efficient solar photochemistry with luminescent solar concentrator based photomicroreactors, Angew. Chem. Int. Ed. 58 (40) (2019) 14374–14378.
[4] H.G. Zhao, F. Rosei, Colloidal quantum dots for solar technologies, Chem 3 (2) (2017) 229–258.
[5] M.G. Debije, P.P.C. Verbunt, Thirty years of luminescent solar concentrator research: solar energy for the built environment, Adv. Energy Mater. 2 (1) (2012) 12–35.
[6] R. Mazzaro, A. Vomiero, The renaissance of luminescent solar concentrators: the role of inorganic nanomaterials, Adv. Energy Mater. 8 (33) (2018) 19.
[7] K.F. Wu, H.B. Li, V.I. Klimov, Tandem luminescent solar concentrators based on engineered quantum dots, Nat. Photonics 12 (2) (2018) 105–110.
[8] C.S. Erickson, L.R. Bradshaw, S. McDowall, J.D. Gilbertson, D.R. Gamelin, D. L. Patrick, Zero-reabsorption doped-nanocrystal luminescent solar concentrators, ACS Nano 8 (4) (2014) 3461–3467.
[9] S.J. Ha, J.H. Kang, D.H. Choi, S.K. Nam, E. Reichmanis, J.H. Moon, Upconversion-assisted dual-band luminescent solar concentrator coupled for high power conversion efficiency photovoltaic systems, ACS Photonics 5 (9) (2018) 3621–3627.
[10] F. Meinardi, F. Bruni, S. Brovelli, Luminescent solar concentrators for building-integrated photovoltaics, Nat. Rev. Mater. 2 (12) (2017) 9.
[11] F. Meinardi, S. Ehrenberg, L. Dhamo, F. Carulli, M. Mauri, F. Bruni, R. Simonutti, U. Kortshagen, S. Brovelli, Highly efficient luminescent solar concentrators based on earth-abundant indirect-bandgap silicon quantum dots, Nat. Photonics 11 (3) (2017) 177–185.
[12] F. Meinardi, A. Colombo, K.A. Velizhanin, R. Simonutti, M. Lorenzon, L. Beverina, R. Viswanatha, V.I. Klimov, S. Brovelli, Large-area luminescent solar concentrators based on 'Stokes-shift-engineered' nanocrystals in a mass-polymerized PMMA matrix, Nat. Photonics 8 (5) (2014) 392–399.
[13] S. Sadeghi, H.B. Jalali, R. Melikov, B.G. Kumar, M.M. Aria, C.W. Ow-Yang, S. Nizamoglu, Stokes-shift-engineered indium phosphide quantum dots for efficient luminescent solar concentrators, ACS Appl. Mater. Interfaces 10 (15) (2018) 12975–12982.
[14] M. Sharma, K. Gungor, A. Yeltik, M. Olutas, B. Guzelturk, Y. Kelestemur, T. Erdem, S. Delikanli, J.R. McBride, H.V. Demir, Near-unity emitting copper-doped colloidal semiconductor quantum wells for luminescent solar concentrators, Adv. Mater. 29 (30) (2017) 10.
[15] L.H. Slooff, E.E. Bende, A.R. Burgers, T. Budel, M. Pravettoni, R.P. Kenny, E. D. Dunlop, A. Buchtemann, A luminescent solar concentrator with 7.1% power conversion efficiency, Phys. Status Solidi-Rapid Res. Lett. 2 (6) (2008) 257–259.
[16] J. Sol, V. Dehm, R. Hecht, F. Wurthner, A. Schenning, M.G. Debije, Temperature-responsive luminescent solar concentrators: tuning energy transfer in a liquid crystalline matrix, Angew. Chem. -Int. Ed. 57 (4) (2018) 1030–1033.

[17] J. Sol, G.H. Timmermans, A.J. van Breugel, A. Schenning, M.G. Debije, Multistate luminescent solar concentrator "smart" windows, Adv. Energy Mater. 8 (12) (2018) 8.
[18] H.J. Song, B.G. Jeong, J. Lim, D.C. Lee, W.K. Bae, V.I. Klimov, Performance limits of luminescent solar concentrators tested with seed/quantum-well quantum dots in a selective-reflector-based optical cavity, Nano Lett. 18 (1) (2018) 395–404.
[19] B.R. Sutherland, Cost competitive luminescent solar concentrators, Joule 2 (2) (2018) 203–204.
[20] J.S. Batchelder, A.H. Zewail, T. Cole, Luminescent solar concentrators.1. theory of operation and techniques for performance evaluation, Appl. Opt. 18 (18) (1979) 3090–3110.
[21] H. Hernandez-Noyola, D.H. Potterveld, R.J. Holt, S.B. Darling, Optimizing luminescent solar concentrator design, Energy Environ. Sci. 5 (2) (2012) 5798–5802.
[22] M.J. Currie, J.K. Mapel, T.D. Heidel, S. Goffri, M.A. Baldo, High-efficiency organic solar concentrators for photovoltaics, Science 321 (5886) (2008) 226–228.
[23] R. Rondao, A.R. Frias, S.F. Correia, L. Fu, V. de Zea Bermudez, P.S. Andre, R. A. Ferreira, L.D. Carlos, High-performance near-infrared luminescent solar concentrators, ACS Appl. Mater. Interfaces 9 (14) (2017) 12540–12546.
[24] B.L. Zhang, P.J. Zhao, L.J. Wilson, J. Subbiah, H.B. Yang, P. Mulvaney, D.J. Jones, K.P. Ghiggino, W.W.H. Wong, High-performance large-area luminescence solar concentrator incorporating a donor-emitter fluorophore system, ACS Energy Lett. 4 (8) (2019) 1839–1844.
[25] F. Corsini, E. Tatsi, A. Colombo, C. Dragonetti, C. Botta, S. Turri, G. Griffini, Highly emissive fluorescent silica-based core/shell nanoparticles for efficient and stable luminescent solar concentrators, Nano Energy 80 (2021).
[26] G. Lyu, J. Kendall, I. Meazzini, E. Preis, S. Baysec, U. Scherf, S. Clement, R. C. Evans, Luminescent solar concentrators based on energy transfer from an aggregation-induced emitter conjugated polymer, ACS Appl. Polym. Mater. 1 (11) (2019) 3039–3047.
[27] S.F. Correia, V. de Zea Bermudez, S.J. Ribeiro, P.S. André, R.A. Ferreira, L. D. Carlos, Luminescent solar concentrators: challenges for lanthanide-based organic–inorganic hybrid materials, J. Mater. Chem. A 2 (16) (2014) 5580–5596.
[28] M.M. Nolasco, P.M. Vaz, V.T. Freitas, P.P. Lima, P.S. André, R.A. Ferreira, P.D. Vaz, P. Ribeiro-Claro, L.D. Carlos, Engineering highly efficient Eu (III)-based tri-ureasil hybrids toward luminescent solar concentrators, J. Mater. Chem. A 1 (25) (2013) 7339–7350.
[29] M.R. Bergren, N.S. Makarov, K. Ramasamy, A. Jackson, R. Guglielmetti, H. McDaniel, High-performance CuInS2 quantum dot laminated glass luminescent solar concentrators for windows, ACS Energy Lett. 3 (3) (2018) 520–525.
[30] X. Gong, H. Jiang, M.Y. Cao, Z.H. Rao, X.J. Zhao, A. Vomiero, Eu-doped ZnO quantum dots with solid-state fluorescence and dual emission for high-performance luminescent solar concentrators, Mater. Chem. Front 5 (12) (2021) 4746–4755.
[31] G.S. Selopal, M. Mohammadnezhad, L.V. Besteiro, O. Cavuslar, J. Liu, H. Zhang, F. Navarro-Pardo, G. Liu, M. Wang, E.G. Durmusoglu, H.Y. Acar, S. Sun, H. Zhao, Z. M. Wang, F. Rosei, Synergistic effect of plasmonic gold nanoparticles decorated carbon nanotubes in quantum Dots/TiO2 for optoelectronic devices, Adv. Sci. (Weinh.) 7 (20) (2020) 2001864.
[32] H. Zhang, L.V. Besteiro, J.B. Liu, C. Wang, G.S. Selopal, Z.S. Chen, D. Barba, Z. M. Wang, H.G. Zhao, G.P. Lopinski, S.H. Sun, F. Rosei, Efficient and stable photoelectrochemical hydrogen generation using optimized colloidal heterostructured quantum dots, Nano Energy (2021) *79*.
[33] H.G. Zhao, D. Benetti, X. Tong, H. Zhang, Y.F. Zhou, G.J. Liu, D.L. Ma, S.H. Sun, Z. M.M. Wang, Y.Q. Wang, F. Rosei, Efficient and stable tandem luminescent solar concentrators based on carbon dots and perovskite quantum dots, Nano Energy 50 (2018) 756–765.
[34] M.Y. Wei, F.P.G. de Arguer, G. Walters, Z.Y. Yang, L.N. Quan, Y. Kim, R. Sabatini, R. Quintero-Bermudez, L. Gao, J.Z. Fan, F.J. Fan, A. Gold-Parker, M.F. Toney, E. H. Sargent, Ultrafast narrowband exciton routing within layered perovskite nanoplatelets enables low-loss luminescent solar concentrators, Nat. Energy 4 (3) (2019) 197–205.
[35] Y. Cheng, L. Ding, Perovskite/Si tandem solar cells: fundamentals, advances, challenges, and novel applications, SusMat 1 (3) (2021) 324–344.
[36] A. Anand, M.L. Zaffalon, G. Gariano, A. Camellini, M. Gandini, R. Brescia, C. Capitani, F. Bruni, V. Pinchetti, M. Zavelani-Rossi, F. Meinardi, S.A. Crooker, S. Brovelli, Evidence for the band-edge exciton of CuInS2 nanocrystals enables record efficient large-area luminescent solar concentrators, Adv. Funct. Mater. 30 (4) (2020) 13.
[37] W.W. Ma, W.J. Li, R.Y. Liu, M.Y. Cao, X.J. Zhao, X. Gong, Carbon dots and AIE molecules for highly efficient tandem luminescent solar concentrators, Chem. Commun. 55 (52) (2019) 7486–7489.
[38] Y.F. Zhou, D. Benetti, X. Tong, L. Jin, Z.M.M. Wang, D.L. Ma, H.G. Zhao, F. Rosei, Colloidal carbon dots based highly stable luminescent solar concentrators, Nano Energy 44 (2018) 378–387.
[39] M.J. Talite, H.Y. Huang, Y.H. Wu, P.G. Sena, K.B. Cai, T.N. Lin, J.L. Shen, W. C. Chou, C.T. Yuan, Greener luminescent solar concentrators with high loading contents based on in situ cross-linked carbon nanodots for enhancing solar energy harvesting and resisting concentration induced quenching, ACS Appl. Mater. Interfaces 10 (40) (2018) 34184–34192.
[40] H.G. Zhao, G.J. Liu, G.T. Han, High-performance laminated luminescent solar concentrators based on colloidal carbon quantum dots, Nanoscale Adv. 1 (12) (2019) 4888–4894.
[41] R. Mazzaro, A. Gradone, S. Angelon, G. Morselli, P.G. Cozzi, F. Romano, A. Vomiero, P. Ceroni, Hybrid silicon nanocrystals for color-neutral and transparent luminescent solar concentrators, ACS Photonics 6 (9) (2019) 2303–2311.
[42] Z. Chen, X. Gu, Y. Guo, X. Wang, M. Shao, B. Dong, Z. Kang, A carbon dot-based total green and self-recoverable solid-state electrochemical cell fully utilizing O2/H2O redox couple, SusMat 1 (3) (2021) 448–457.
[43] H.G. Zhao, Refractive index dependent optical property of carbon dots integrated luminescent solar concentrators, J. Lumines 211 (2019) 150–156.
[44] M.J. Talite, H.Y. Huang, K.B. Cai, K.C.C. Co, P.A.C. Santoso, S.H. Chang, W. C. Chou, C.T. Yuan, Visible-transparent luminescent solar concentrators based on carbon nanodots in the siloxane matrix with ultrahigh quantum yields and optical transparency at high-loading contents, J. Phys. Chem. Lett. 11 (2) (2020) 567–573.
[45] Y.X. Li, P. Miao, W. Zhou, X. Gong, X.J. Zhao, N-doped carbon-dots for luminescent solar concentrators, J. Mater. Chem. A 5 (40) (2017) 21452–21459.
[46] F. Mateen, M. Ali, H. Oh, S.-K. Hong, Nitrogen-doped carbon quantum dot based luminescent solar concentrator coupled with polymer dispersed liquid crystal device for smart management of solar spectrum, Sol. Energy 178 (2019) 48–55.
[47] H.G. Zhao, G.J. Liu, S.J. You, F.V.A. Camargo, M. Zavelani-Rossi, X.H. Wang, C. C. Sun, B. Liu, Y.M. Zhang, G.T. Han, A. Vomiero, X. Gong, Gram-scale synthesis of carbon quantum dots with a large Stokes shift for the fabrication of eco-friendly and high-efficiency luminescent solar concentrators, Energy Environ. Sci. 14 (1) (2021) 12.
[48] Z. Wang, F. Yuan, X. Li, Y. Li, H. Zhong, L. Fan, S. Yang, 53% efficient red emissive carbon quantum dots for high color rendering and stable warm white-light-emitting diodes, Adv. Mater. 29 (2017) 37.
[49] P. Ma, X. Sun, W. Pan, G. Yu, J. Wang, Green and orange emissive carbon dots with high quantum yields dispersed in matrices for phosphor-based white LEDs, ACS Sustain. Chem. Eng. 8 (8) (2020) 3151–3161.
[50] Z. Sun, W. Zhou, J. Luo, J. Fan, Z.C. Wu, H. Zhu, J. Huang, X. Zhang, High-efficient and pH-sensitive orange luminescence from silicon-doped carbon dots for information encryption and bio-imaging, J. Colloid Interface Sci. 607 (Pt 1) (2022) 16–23.
[51] J. Chen, W.-R. Liu, Y. Li, X. Zou, W. Li, J. Liang, H. Zhang, Y. Liu, X. Zhang, C. Hu, B. Lei, Architecting ultra-bright silanized carbon dots by alleviating the spin-orbit coupling effect: a specific fluorescent nanoprobe to label dead cells, Chem. Eng. J. 428 (2022).
[52] L.Z. Sui, W.W. Jin, S.Y. Li, D.L. Liu, Y.F. Jiang, A.M. Chen, H. Liu, Y. Shi, D.J. Ding, M.X. Jin, Ultrafast carrier dynamics of carbon nanodots in different pH environments, Phys. Chem. Chem. Phys. 18 (5) (2016) 3838–3845.
[53] Z. Qian, X. Shan, L. Chai, J. Ma, J. Chen, H. Feng, Si-doped carbon quantum dots: a facile and general preparation strategy, bioimaging application, and multifunctional sensor, ACS Appl. Mater. Interfaces 6 (9) (2014) 6797–6805.
[54] C. Yang, J. Zhang, W.T. Peng, W. Sheng, D. Liu, P.S. Kuttipillai, M. Young, M. R. Donahue, B.G. Levine, B. Borhan, R.R. Lunt, Impact of stokes shift on the performance of near-infrared harvesting transparent luminescent solar concentrators, Sci. Rep. 8 (1) (2018) 16359.
[55] Y. Chen, M. Zheng, Y. Xiao, H. Dong, H. Zhang, J. Zhuang, H. Hu, B. Lei, Y. Liu, A self-quenching-resistant carbon-dot powder with tunable solid-state fluorescence and construction of dual-fluorescence morphologies for white light-emission, Adv. Mater. 28 (2) (2016) 312–318.
[56] J. He, Y. He, Y. Chen, B. Lei, J. Zhuang, Y. Xiao, Y. Liang, M. Zheng, H. Zhang, Y. Liu, Solid-state carbon dots with red fluorescence and efficient construction of dual-fluorescence morphologies, Small 13 (26) (2017).
[57] Z. Zhou, P. Tian, X. Liu, S. Mei, D. Zhou, D. Li, P. Jing, W. Zhang, R. Guo, S. Qu, A. L. Rogach, Hydrogen peroxide-treated carbon dot phosphor with a bathochromic-shifted, aggregation-enhanced emission for light-emitting devices and visible light communication, Adv. Sci. (Weinh.) 5 (8) (2018) 1800369.
[58] C.C. Yang, H.A. Atwater, M.A. Baldo, D. Baran, C.J. Barile, M.C. Barr, M. Bates, M. G. Bawendi, M.R. Bergren, B. Borhan, C.J. Brabec, S. Brovelli, V. Bulovic, P. Ceroni, M.G. Debije, J.M. Delgado-Sanchez, W.J. Dong, P.M. Duxbury, R.C. Evans, S. R. Forrest, D.R. Gamelin, N.C. Giebink, X. Gong, G. Griffini, F. Guo, C.K. Herrera, A. W.Y. Ho-Baillie, R.J. Holmes, S.K. Hong, T. Kirchartz, B.G. Levine, H.B. Li, Y.L. Li, D.Y. Liu, M.A. Loi, C.K. Luscombe, N.S. Makarov, F. Mateen, R. Mazzaro, H. McDaniel, M.D. McGehee, F. Meinardi, A. Menendez-Velazquez, J. Min, D. B. Mitzi, M. Moemeni, J.H. Moon, A. Nattestad, M.K. Nazeeruddin, A.F. Nogueira, U.W. Paetzold, D.L. Patrick, A. Pucci, B.P. Rand, E. Reichmanis, B.S. Richards, J. Roncali, F. Rosei, T.W. Schmidt, F. So, C.C. Tu, A. Vahdani, W.G.J.H.M. van Sark, R. Verduzco, A. Vomiero, W.W.H. Wong, K.F. Wu, H.L. Yip, X.W. Zhang, H.G. Zhao, R.R. Lunt, Consensus statement: standardized reporting of power-producing luminescent solar concentrator performance, Joule 6 (1) (2022) 8–15.
[59] V.I. Klimov, T.A. Baker, J. Lim, K.A. Velizhanin, H. McDaniel, Quality factor of luminescent solar concentrators and practical concentration limits attainable with semiconductor quantum dots, ACS Photonics 3 (6) (2016) 1138–1148.